Zinc speciation in fly ash from MSWI using XAS - novel insights and implications

(article starts on next page)

Zinc speciation in fly ash from MSWI using XAS - novel insights and implications

Jenny Rissler [a,b,c,*], Karin Karlfeldt Fedje [d,e], Konstantin Klementiev [f], Burçak Ebin [g], Charlotte Nilsson [h], Haakon M. Rui [i], Tone M. Klufthaugen [i], Simone Sala [c], Inge Johansson [i]

[a] Ergonomics and Aerosol Technology, Lund University, SE-22100 Lund, Sweden
[b] NanoLund, Lund University, SE-22100 Lund, Sweden
[c] RISE Research Institutes of Sweden, SE-22370 Lund, Sweden
[d] Recycling and Waste Management, Renova AB, Box 156, SE-401 22 Gothenburg, Sweden
[e] Department of Architecture and Civil Engineering, Chalmers University of Technology, SE-412 96 Gothenburg, Sweden
[f] MAX IV Laboratory, Lund University, SE-22100 Lund, Sweden
[g] Nuclear Chemistry and Industrial Material Recycling, Chalmers University of Technology, SE-412 96 Gothenburg, Sweden
[h] Fortum Waste Solutions AB, SE-69285 Kumla, Sweden
[i] NOAH AS, 3081 Holmestrand, Norway

HIGHLIGHTS

- Zinc speciation in MSWI fly ash was studied with XAS, analyzed using 32 references.
- Evidence for the formation of potassium zinc chloride salt (K2ZnCl4).
- Other zinc bearing forms are silicates, ferrite, aluminate, surface adsorbed zinc and hydrozinkite.
- K2ZnCl4 is the dominating zinc form in grate-fired boiler ash, while zinc in spinel forms in CFB ash.
- The K2ZnCl4 is hydroxylated during dry storage and in the XAS sample preparation.

GRAPHICAL ABSTRACT
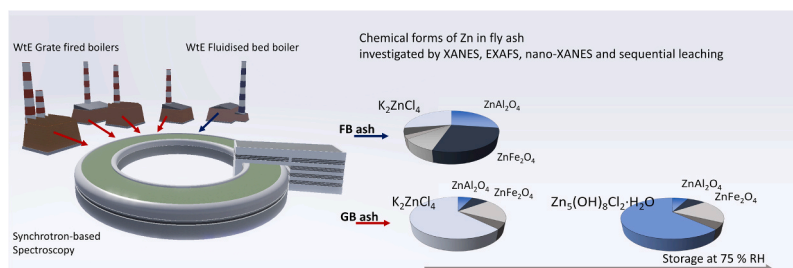
ARTICLE INFO

ABSTRACT

The chemical forms of zinc in fly ash from municipal solid waste incineration (MSWI) crucially affect ash management, influencing both material recovery options and the risk of unwanted leaching into ecosystems. The zinc speciation was investigated in fly ash samples sourced from full-scale MSWI plants, including four grate fired boilers (GB) and one fluidized bed boiler (FB). We applied X-ray Absorption Spectroscopy (XAS), and the spectra were analyzed against a unique library of over 30 relevant compounds, tailored to the nuances of zinc chemistry of fly ash. Nano-XANES and sequential leaching were employed as complementary analytical methods. Multiple chemical forms of zinc were found in the ash, whereof potassium zinc chloride salts (K_2ZnCl_4) emerged as the predominant form in GB fly ash representing 41–64 % of the zinc content, while less for FB fly ash (19 %). The mere exposure to humidity in the air during storage resulted in hydroxylation of the alkali zinc chlorides into $Zn_5(OH)_8Cl_2 \cdot H_2O$. Other forms of zinc in the ash were $Zn_4Si_2O_7(OH)_2 \cdot H_2O$, $ZnFe_2O_4$, $ZnAl_2O_4$, surface adsorbed

zinc, and $Zn_5(CO_3)_2(OH)_6$. Notably, the proportion of zinc in spinel forms ($ZnFe_2O_4$ and $ZnAl_2O_4$) increased threefold in FB ash compared to GB ash, representing ~60 % and ~10–20 % of the zinc, respectively.

1. Introduction

As urbanization intensifies and industrial activities expand, the generation of waste has escalated, and is foreseen to continue to increase. As a result, waste incineration has doubled in EU the last 25 years [1]. Waste-to-energy (WtE) incineration is an efficient way to treat and utilize waste. Besides energy recovery from the material, producing both electricity and heat, the treatment leads to an efficient volume and mass reduction, as well as degradation of organic pollutants and toxins in the waste. Remaining after the incineration are the predominately inorganic ashes: bottom and fly ash. Depending on the volatility of the metals or their corresponding compounds, some metals accumulate in the fly ash, while others are mainly found in the bottom ash (e.g. [2]). Examples of metals that are enriched in fly ash, often present in significant concentrations i.e. up to a few percent, are copper, lead, and zinc [3], but the variations in concentrations are large [4].

The European Commission has recently presented an updated critical raw materials list, specifically recommending the utilization of secondary raw materials to secure the metal supply of today's society, including zinc [5]. While the potentially toxic elements present in ashes from WtE incineration pose environmental challenges when handling and using the ash as a secondary resource, they also offer the potential for material recovery and reclamation as secondary products [3,6]. Zinc, used in a variety of products from galvanization to cosmetics and alloys, has been in the focus of resource recovery (Zhang el at., 2021) with a few full-scale plants recently employing zinc extraction [7-9]. Despite the variety in recovery approaches, a complete mobilization of zinc remains unachieved, highlighting the need for further advancements in the speciation of zinc [8-11].

The speciation of zinc is a key factor when understanding its mobilization from ash, which is crucial for developing more efficient recovery methods and ensuring the safe use of stabilized ash, and when evaluating the risk of toxic compounds in the ash to leach into the environment. Moreover, comprehending how zinc speciates during the formation of the fly ash could facilitate new innovative approaches for smarter particle traps or fuel mixture. However, the knowledge of the chemical forms of transition metals in fly ash particles remains limited. This limitation is attributed not only to the relatively low concentrations but also to the intricate nature of the ash matrix, which comprises numerous elements in diverse chemical forms, including both amorphous and crystalline phases. Consequently, conventional methods have limited efficacy.

In the realm of analytical techniques for metal speciation in complex materials such as WtE incineration ash, a promising technique is X-ray Absorption Spectroscopy (XAS), which includes both X-ray Absorption Near Edge Structure (XANES) and Extended X-ray Absorption Fine Structure (EXAFS). Zhang et al. [3] As XAS is element-specific, this advanced method can home in on specific low-content constituents within complex matrices, revealing detailed information about their local chemical environment, oxidation state, coordination environment, and bond lengths, also for amorphous structures. [12,13] In the context of WtE ash research, this capability is crucial as it allows to ascertain the speciation of metals in low amounts in the heterogeneous ash. Thereby XAS contributes to a deeper understanding the formation of zinc species in the ash, paving the way for optimised material recovery and safe secondary use. Several earlier studies have applied XAS to investigate metal speciation in MSWI fly ash, whereof most studies have been focused on Pb, Cu, Zn and Sb (e.g. [14-20]). A more detailed overview of earlier XAS studies of zinc in ash is given in the discussion.

XANES is a fingerprint technique, with spectral interpretation generally requiring comparisons to empirical XANES spectra of known compounds [21]. To identify and quantify chemical forms of metals in the ash, XANES spectra are often analyzed using linear combination fitting (LCF) using a set of reference spectra [3]. While XANES is an extremely powerful method for determining metal speciation in ash, unequivocal identification and quantification of specific species require a comprehensive library of relevant reference spectra [16]. Apart from this, it is often advisable to corroborate XANES results using complementary analytical techniques, a practice omitted in many previous studies which also typically relies on a limited library of XANES reference spectra.

In the present study we investigate the chemical forms of zinc in fly ash samples collected from five full-scale WtE incineration plants. This involves ash from four grate-fired boilers (GB), the predominant technology in WtE incineration, and for comparison one ash from a fluidized bed boiler (FB). The primary analytical method applied is XANES. The XANES spectra are analyzed through linear combination fitting (LCF) with a, for the purpose curated database of zinc references. The unique database encompasses over 30 compounds, tailored to the nuances of zinc chemistry within the specific context of fly ash, thereby enhancing the precision and relevance of the XANES analysis. Furthermore, to secure the correctness of the results, the LCF is done using two different approaches, and results are compared to those from EXAFS, nano-XANES (offering 50 nm x 50 nm 2D spatial resolution), and sequential leaching experiments. Additionally, we examine chemical transformations occurring in the ash under different storage conditions.

2. Materials and methods

2.1. Ash samples

Fly ash samples were collected from five different full-scale WtE incineration plants in Sweden, Norway, and Denmark, which all incinerate a combination of municipal and industrial waste. One sample (FB1) originates from fluidized bed incineration, while the other four samples are from grate fired combustors (GB2–5). The FB1 ash was collected from the fabric filters placed after the alkaline scrubbers and the addition of activated carbon. All GB ash samples originate from the dry electrostatic precipitators (ESP) used for particle removal. Ash samples GB3 and GB4 were collected from the ash silos, while GB2 and GB5 were collected directly from the hoppers. All ash samples were collected during normal and stable incineration conditions to ensure representative samples, and at the same time of year (Jan-Mars). After collection, the samples were packed in dry and airtight containers until analysis.

2.2. Elemental content

Elemental characterization of the original ash samples was done via digestion and analysis with Inductively coupled plasma sector field mass spectrometry (ICP-SFMS), using ASTM D3682, ASTM D4503–08 (digestion using lithium metaborate ($LiBO_2$) and HNO_3) and SS-EN-13656 (digestion with HF, HNO_3, and HCl). The concentrations of selected elements are given in Table 1. The zinc contents in the ashes were between 2 and 4 wt% in the GB ashes (GB2-GB5), while less than 1 % in FB1.

na: not analysed.

2.3. X-ray absorption spectroscopy (XAS)

XAS measurements were carried out at the beamline Balder, placed at the 3.0 GeV ring at MAX IV Laboratory [22]. The 3.0 GeV ring

Table 1
Contents of selected elements in original ash samples FB1 and GB2–5. All amounts are provided in mg/kg (dry weight).

	FB1	GB2	GB3	GB4	GB5
	Major elements				
Al	85 200	37 500	48 500	27 900	23 400
Ca	210 000	157 000	172 000	149 000	122 000
Fe	33 300	21 300	18 100	15 900	9 850
K	13 700	42 000	49 000	64 000	72 600
Mg	17 400	14 600	16 400	11 900	10 000
Na	18 400	50 400	54 000	42 100	81 000
P	3 900	5 750	9 330	6 700	5 410
S	31 700	55 900	39 300	68 900	63 500
Si	111 000	124 000	94 200	140 000	53 200
Ti	11 600	11 300	13 400	6 770	7 320
Zn	*8 030*	*20 700*	*20 600*	*19 700*	*40 300*
	Minor elements				
As	30.3	115	175	280	1 410
Ba	2 540	3 860	2 480	1 610	1 340
Cd	28	106	137	174	256
Co	79.2	97.7	27.2	16.4	25.9
Cr	386	616	431	306	558
Cu	6 010	2 000	1 760	766	2 560
Hg	1.8	0.3	1.2	< 0.05	0.8
Mn	1 270	1 030	2 230	1 050	563
Mo	26	55	19	12	29
Ni	219	155	114	41	127
Pb	2 460	4 410	3 540	3 020	4 560
Sb	355	2 300	1 260	1 150	2 070
Sn	176	772	668	692	1 530
Sr	508	439	476	504	299
V	89	129	58	57	38
	Anions				
Br	918	1 440	2 240	1 250	4 620
Cl	78 900	85 400	127 000	48 800	213 000
F	580	1 730	510	880	na

operates at ~400 mA. A beam size of ~200 × 100 μm was used for ash samples while focused down to ~70 × 70 μm for the references. The energy given by the monochromator (pair of cryogenically cooled Si111 crystals) was calibrated by assigning the first peak of the first derivative for the K-edge of a zinc reference foil to 9659 eV. XANES and EXAFS are both included in XAS, for which different energy ranges of the XAS spectra are measured and analyzed. XANES and EXAFS spectra of both ash samples and reference substances were recorded in transmission mode using gas-filled ionization chambers, scanning the K-edge of zinc. A step size of 0.2 eV was used. For the ash samples, the beam position was moved 0.2 mm between each scan, mitigating possible radiation damage and the final spectra composed of 3–6 merged scans. EXAFS spectra were measured using the same beamline and setting, but with a longer acquisition time (1 min vs 15 s) and a broader energy interval (up to 1200 eV above the edge compared to 250 eV). XANES ash spectra were pre-processed and analyzed using the ATHENA software package [23] and EXAFS analyzed using VIPER [24]. XANES scans were performed for all samples, and for three samples also EXAFS (GB4, GB5 and the GB4 ash stored at 75 % Relative Humidity for 5 months, see Section 2.6).

Fourier transformed (FT) EXAFS spectra resemble the radial atomic distribution function but the peaks in this distribution are shifted toward smaller distances. The magnitude of this shift depends on the atomic nature of the respective coordination shell. Long-range ordering is manifested in EXAFS as high frequency contributions, visible as peaks on FT EXAFS at large distances; additionally, FT EXAFS peaks of highly ordered atomic shells are narrow and, reversely, disordered shells have broadened FT contributions.

The samples and reference compounds were prepared by mixing with boron nitride in a mortar and pressed into 13-mm-diameter tablets, aiming for an optical thickness of the tablet of 2–2.5. The sample preparation was performed according to standard procedures for XAS. The reproducibility of preparing new tablets for the same type of ash

samples was tested in an earlier study [16] and to some extent also during the current study.

The possible effect of sample preparation on the chemical form of zinc (mixing in a mortar with a binder and press into tablets) was investigated measuring an ash sample taped to the sample holder. As expected, the XANES spectra of the taped sample had a higher noise level, but the shape of the spectra was unchanged compared to the pressed tablet, when performing the measurements < 6 h prior to the sample preparation. However, upon re-measuring the same prepared tablet 1–2 months following its initial preparation, a noticeable change in the chemical form of zinc was observed over time, as detailed in Section 2.6.

2.3.1. Reference compounds for XAS

The selection of references developed and included in the present study is based on an extended literature review. Commercially available compounds were purchased (>99 % purity), and references identified as relevant for waste incineration ash, not available commercially, were synthesized in the lab. Apart from specific zinc compounds, references representing zinc adsorbed to the surfaces of other compounds were synthesized.

A full list of references is found in Supplementary Information (SI), Table S1, including details about origin (commercially available or synthesized for the purpose) and of the synthesized references. The pure compounds included in the analysis are $KZnCl_3$, K_2ZnCl_4, $CaZnCl_4$, $ZnCl_2$, $Zn_5(OH)_8Cl_2 \cdot H_2O$, $ZnBr_2$, ZnO, $Zn(OH)_2$, Zn_2O, $ZnOOH$, $Zn_3(PO_4)_2 \cdot 4 \ H_2O$, $ZnNO_3 \cdot 6 \ H_2O$, $Zn_5(CO_3)_2(OH)_6$, $ZnCO_3$, $ZnSO_4 \cdot H_2O$, ZnS, $Zn_4Si_2O_7(OH)_2 \cdot H_2O$, Zn_2SiO_4, $Ca_2ZnSi_2O_7$, $CuZnFe_2O_4$ (nano form), $ZnFe_2O_4$, $ZnAl_2O_4$, metallic Zn, Cu_4Zn_6, $ZnSb_2O_6$, $ZnTiO_2$, and $Zn_{1-x}Al_x(OH)_2[SO_4]_x/2 \cdot nH_2O$. $CaZnCl_4$ is a synthesized reference with a structure that stoichiometrically should be $CaZnCl_4$, but since this compound is not included in the X-ray Diffraction (XRD) database this could not be confirmed. The reference is produced from $CaCl_2$ and $ZnCl_2$ and the processed reference differed from the XRD spectra of both $CaCl_2$ and $ZnCl_2$. Furthermore, the Zn XANES spectra of the reference was clearly deviant from $ZnCl_2$ and more closely resembled that of $KZnCl_3$ and K_2ZnCl_4.

Three references representing zinc adsorbed to surfaces were prepared: $Zn\_Fe_{10}O_{14}(OH)_2$, $Zn\_Al_2O_3 \cdot 4 \ SiO_4 \cdot H_2O$, Zn_CaCO_3, and Zn_CaSO_4, where "Zn_" is used indicating that zinc is adsorbed. For $Zn\_Fe_{10}O_{14}(OH)_2$ a color change was observed, possibly indicating that cation exchange had taken place.

The purities of all references were controlled using XRD, and adsorbed Zn amounts were analyzed by inductively coupled plasma optical emission spectroscopy (ICP-OES), given in SI, Table S1. A handful of the synthesized references were discarded after the XRD analysis due to impurities.

2.3.2. Linear combination fitting of XANES spectra

To determine the abundance and relative proportions of various zinc forms, the XANES spectra from the ash samples were analyzed using linear combination fitting (LCF). This LCF utilized XANES spectra from reference compounds listed in Section 2.3.2 and in Table S1, measured at the same beamline. The energy interval used for the LCF was 25 eV and 35 eV below and above the absorption edge, respectively.

The robustness of the results were further tested by also fitting the derivative of the XANES spectra, which highlights other spectral features than the normalized spectra. The absence of important references can be evidenced by significant deviations in the results from each respective approach. The results from fitting the normalized spectra is are considered the primary outcome of the analysis as this is the standard practice.

Previous blind tests have shown that LCF predictions for compound presence below 3–4 % are highly uncertain [16]. Consequently, any compound fitted at less than 4 % was disregarded. This approach aligns with recommendations from other studies utilizing LCF for XANES data

analysis [25]. The fitting procedure used involved iteratively removing the least abundant compound until each zinc compound in the fit accounted for at least 5 %.

2.4. Nanoscale XANES

Nanoscale XANES (nano-XANES) measurements were carried out at I14, the hard X-ray nanoprobe beamline at Diamond Light Source, UK [26]. The beamline is optimized for scanning microscopy and was operated with a focused X-ray beam, achieving a focal spot size of 50 nm. An array of 4 silicon drift detectors (SDD) is positioned 17 mm upstream the sample and records X-ray fluorescence emission in back-scatter geometry while an area detector downstream the sample records X-ray scattering. In this experiment, overview images were obtained for each sample based on fluorescence signal. Then, nano-XANES measurements were carried out on single points (denoted point nano-XANES) or small regions of interest (ROIs) selected based on the overview images. For each nano-XANES acquisition, several fluorescence maps of the same area were collected at 152 different incident photon energies around the K-edge of zinc (~ 9.7 keV): a variable energy step size was used such that it was as large as 6–8 eV far from the absorption edge and 0.5 eV near the feature-rich region around the absorption edge. Nano-XANES data were analyzed in ATHENA [23].

Samples were prepared by dispersing the ash particles into air in a closed vial by a pulse of pressurized air. The aerosol was introduced into a Nanometer Aerosol Sampler (TSI Model 3089) where the particles were deposited by electrostatic precipitation on 1-μm-thick silicon nitride membranes supported on silicon frames (window size 2.0 mm × 2.0 mm, Norcada NX5200F), using an electrical field of 9500 V. The aerosol was also led into a chamber where the particles were given time to sediment onto the silicon nitride membranes, allowing sampling of larger particles.

20 point nano-XANES spectra were recorded using a 50 nm beam (4 spectra per sample type for FB1, GB3 and GB5, while 8 for GB2, and none for GB4). For the point nano-XANES spectra, zinc-rich spots were identified, typically in particles larger than 2–3 μm. Thus, these spectra should not be regarded as statistically representative for the entire ash.

2.5. Sequential leaching

Sequential extraction was performed according to a modified version [27] of the procedure developed by Tessier et al. [28]. Briefly, samples of the ashes were extracted in five consecutive steps using increasingly aggressive extractants. The solid and liquid phases were separated by centrifugation (4000 RPM, 10 min), rinsed with de-ionized water (18.2 MΩ) and centrifuged a second time to remove the rinsing water, before being transferred to the subsequent step in the sequence. The extractants used were: i) de-ionized water (18.2 MΩ) ("MQ"); ii) 1 M $NH_4CH_3CO_2$, pH 7 ("Ac7"); iii) 1 M $NH_4CH_3CO_2$, pH 5 ("Ac5"); iv) 0.04 M $NH_2OH \cdot HCl$ in 25 % CH_3COOH ("Red"); v_a) 0.02 M HNO_3 and 30 % H_2O_2; v_b) 3.2 M $NH_4CH_3CO_2$ in 20 % HNO_3 ("Ox"). All extractions were done with a liquid:solid ratio of 10, preparation of all solutions was done using de-ionized water (18.2 MΩ) and analytical grade chemicals.

2.6. Laboratory study of the effect of storage of ash on zinc speciation

This test was prompted by observed changes in the zinc XANES spectra when re-measuring the same tablets at a later occasion, suggesting a chemical transformation of the zinc during storage of the prepared samples. In the test, sub samples of GB4 ash were stored for five months at six different conditions all at room temperature: in a full-packed closed vial (i), in an atmosphere of N_2 (ii), in dry air (iii) (<20 %), in indoor air before and after grinding (iv and v), and in air with 75 % RH (vi). For the latter, the RH was controlled to 75 % by a saturated solution of NaCl stored in the same container as the ash [29].

The purpose of the test was to discern the potential effects of

exposure to oxygen (i vs ii), humidity (i vs vi), and the effect of creating new exposed surfaces when grinding the ash in the sample preparation procedure (iii vs iv). For the experiments, ash from GB4 was used, motivated by that the observed change in the XANES spectra were most prominent for the GB ashes, and that all GB ashes followed the same trend.

3. Results and discussion

3.1. XANES first order analysis

For all examined ash samples, the energy at the absorption edge was ~ 9661.9 eV, indicating that the zinc oxidation state was + 2 for all samples. The absorption edge is here defined as the energy where the normalized spectra reach 0.5. The XANES spectra of the GB ashes displayed a high degree of similarity, suggesting the presence of analogous zinc forms in these samples. Contrastingly, the XANES spectrum of the fluidized bed ash (FB1) showed notable differences, implying a different zinc speciation. XANES spectra of all samples are shown in Fig. 1a.

All XANES spectra have four characteristic peaks/spectral features, with three peaks close to the edge: at 9664.4 eV, 9668 eV, and 9673 eV (2.5 eV, 6.1 eV, and 11.1 eV above the absorption edge), and a broader feature around 9685.5 eV (23.6 eV above the absorption edge), indicated with dashed lines in Fig. 1. For the FB ash, the relative intensities of the three first peaks are different compared to the GB ashes, with pronounced peaks around 9664.4 eV and 9673 eV resembling the structures found in the XANES spectra of $ZnAl_2O_4$ and $ZnFe_2O_4$, Fig. 1b. The first peak above the absorption edge, found in all GB ashes, agrees well with the dominating peak of the alkali zinc chloride salts (K_2ZnCl_4, $KZnCl_3$, and $CaZnCl_4$) (see Figs. 1b and 2).

3.2. Zinc speciation (linear combination fitting of XANES data)

The current study surpasses previous XANES research on MSWI ash by incorporating the most extensive library of references to date, consisting of 32 XANES reference spectra. The XANES spectra of the references used for the linear combination fitting (LCF) are depicted in Fig. 2. The XANES fits closely resembles the measured spectra, with the most significant deviation noted in the fluidized bed sample (FB1). Measured XANES spectra, along with the fits, are shown in Fig. 1a. In Fig. 1b the XANES spectra of the most commonly occurring references in the LCF are shown.

Out of the 32 references, a few compounds consistently appear in the LCF, all representing zinc in oxidation state + 2. The most common zinc-forms are of two types: spinels ($ZnAl_2O_4$ and $ZnFe_2O_4$) and potassium zinc chloride salts, likely K_2ZnCl_4. Apart from these compounds also hemimorphite ($Zn_4Si_2O_7(OH)_2 \cdot H_2O$), hydrozincite ($Zn_5(CO_3)_2(OH)_6$), and Zn^{2+} adsorbed to ferrihydrite was found present. For the FB1 sample, phosphate ($Zn_3(PO_4)_2$) was also predicted. The results from the LCF are presented in Table 3 and Fig. 3, grouped into types of compounds with similar properties from a solubility perspective, and with similarities in XANES features. Results from the LCF, divided into each compound, are found in the SI, Table S2. Note that in the results (Table 3, Table S2 and Fig. 3), the molar percentage of zinc in each chemical form is given, e.g. 22 % of all Zn in FB1 is present as $Zn_3(PO_4)_2$.

Table 2

Overview of the experiment on the effect of storage conditions on zinc speciation.

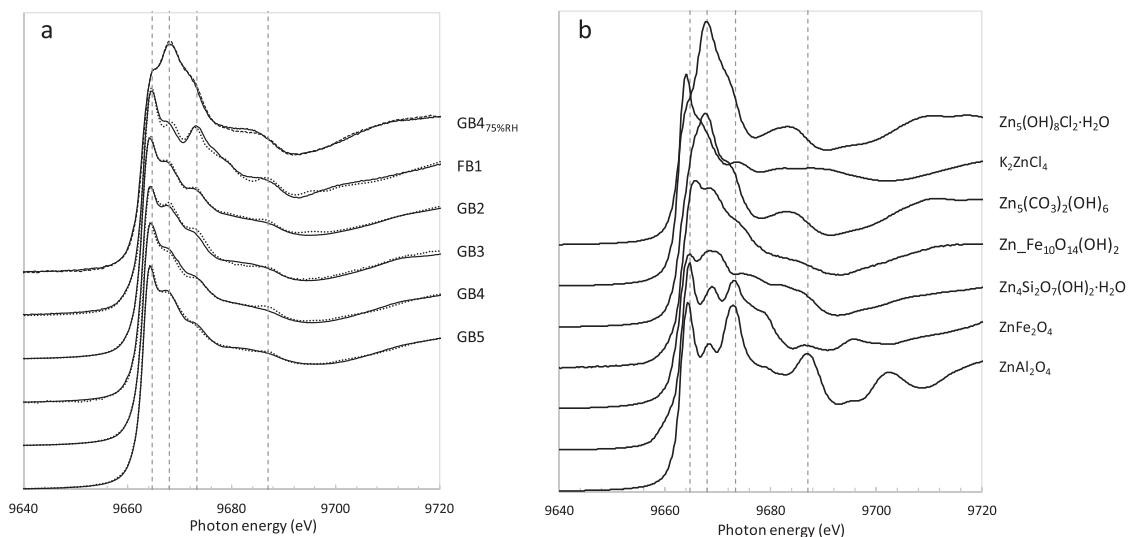| Storage (5 months)		Sample name
Close-packed in sealed vial	(i)	GB4
In N_2	(ii)	GB4_N_2
In air at < 20 % RH	(iii)	GB4_< 20 % RH
Open vial in room air	(iv)	GB4_open
Ground, open vial in room air	(v)	GB4_open_gr
In air at 75 % RH	(vi)	GB4_75 % RH

Fig. 1. a) XANES spectra at the zinc K-edge for all ash samples. The dotted lines show the result from the linear combination fitting. b) XANES spectra of a selection of the most frequently occurring forms according to LCF for reference. The dashed vertical grey lines indicate the four typical features found in the spectra.
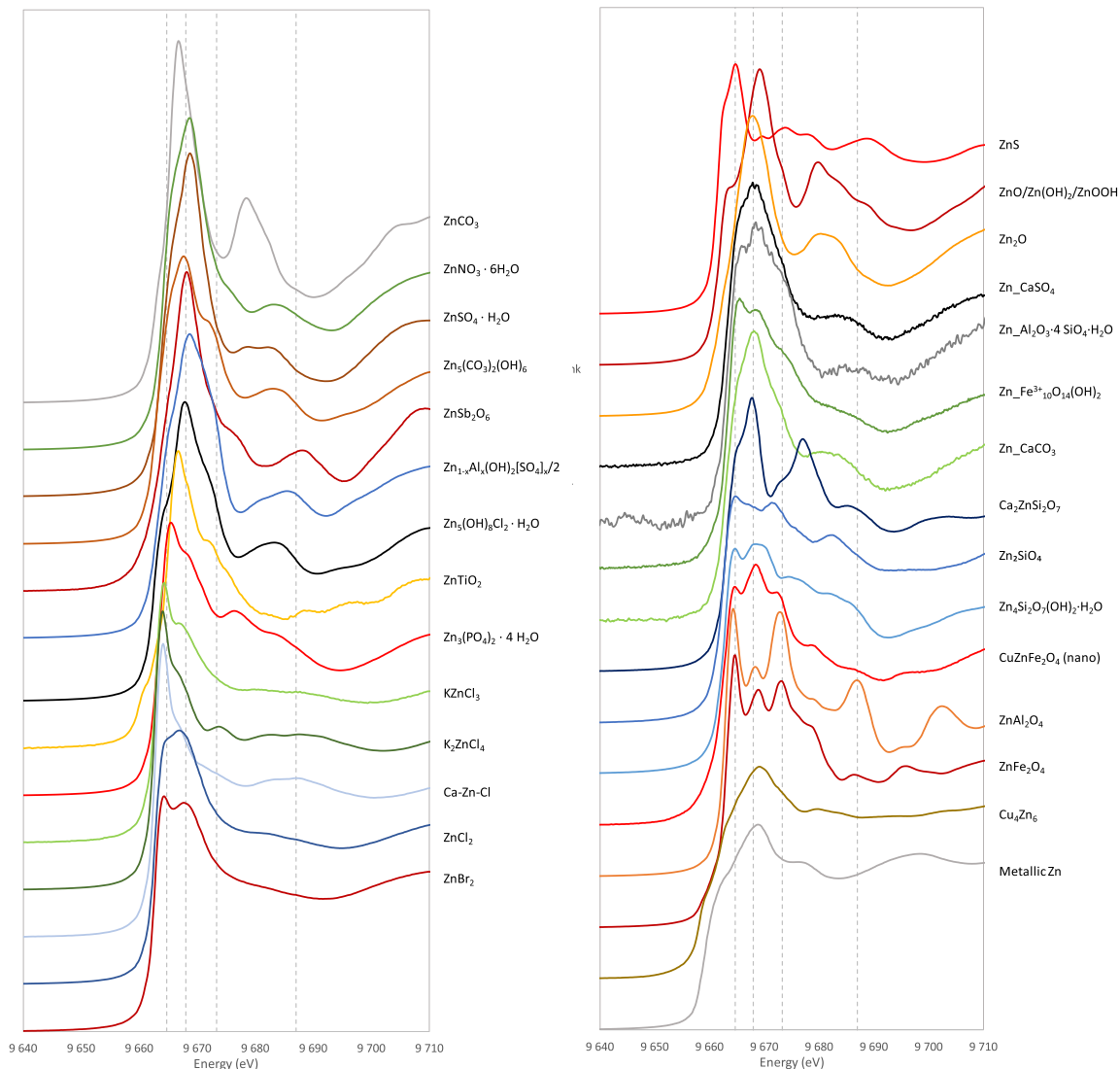

Fig. 2. Overview of XANES spectra of zinc references included in the analysis by linear combination fitting.

Table 3

The resulting zinc speciation from LCF of reference XANES spectra to XANES spectra of the ash samples. The interval fitted was −25 eV to + 35 eV, where 0 eV corresponded to the absorption edge. The numbers given in the table are the molar percentage of zinc bound in the respective chemical form.

	FB1	GB2	GB3	GB4	GB5
Spinels ($ZnAl_2O_4$ / $ZnFe2O4$)	59 %	21 %	17 %	14 %	10 %
K_xZnCl_x	19 %	45 %	41 %	51 %	64 %
$Zn_4Si_2O_7(OH)_2 \cdot H_2O$	< 5 %	20 %	17 %	12 %	11 %
Adsorbed Zn	< 5 %	< 5 %	17 %	22 %	14 %
$Zn_5(CO_3)_2(OH)_6$	< 5 %	14 %	7 %	< 5 %	< 5 %
$Zn_3(PO_4)_2$	22 %	< 5 %	< 5 %	< 5 %	< 5 %

The FB ash had the highest predicted content of spinels ($ZnAl_2O_4$ / $ZnFe_2O_4$), in total ~60 % compared to typically 10–20 % for the GB ash. This can explain the characteristic difference in the XANES spectra between the GB ashes and the FB ash where the latter has more pronounced peaks at 9664.4 eV and 9673 eV (Fig. 1). When fitting the derivate of the FB1 ash XANES spectra, the predicted fraction of zinc bound in the form of spinels was predicted to be lower (~40 %). Instead, the LCF of the derivative suggests that 20 % of the zinc is associated with ferrihydrite, not predicted to be present for the LCF of the XANES spectra. The difference indicate that some reference compound is missing for this type of ash.

The XANES spectra of K_2ZnCl_4, $KZnCl_3$, and $CaZnCl_4$ are all very similar. In the final LCF, $CaZnCl_4$ was excluded, motivated by the fact that the LCF was as good with as without including this compound and that the precise chemical form of this specific reference could not be identified with XRD. Excluding $CaZnCl_4$ from the fit, the total fraction of zinc bound in alkali salts was preserved in the fit (± 3 %). If including the $CaZnCl_4$ system in the fit, a minor fraction of this system was predicted for all samples except GB2. To further elucidate which alkali zinc chloride salt is present in ash, XRD measurements were performed for the sample with the highest predicted content of alkali zinc chloride salts (i.e. GB5). The results showed peaks in the XRD spectrum agreeing well with those of K_2ZnCl_4, while not of $KZnCl_3$. Thus, the alkali zinc chloride salt in the ash is very likely K_2ZnCl_4. This agrees with two earlier studies also reporting the presence of alkali zinc chloride salts [30,31]. The three alkali zinc chlorides here mentioned are highly soluble and all represent easily recoverable zinc.

When conducting meticulous measurements, the primary uncertainty in linear combination fitting (LCF) lies in the necessity to include relevant references. Furthermore, nanoscale variations of the chemical environment for zinc may induce distortions in the XANES spectra [32]. Out of the 32 references, LCF consistently predicted the presence of the same set of compounds in the ash samples which supports the robustness of the fits. To further test the robustness of the LCF, also the derivative of the XANES spectra were fitted and the results from respective approach compared, see Fig. 3 and Table S2 (SI). For the GB ashes, both approaches consistently identified the same zinc compounds, albeit in slightly different proportions. Given the substantial number of references in the LCF, this reinforces our confidence in the robustness of the fits. The variance in the proportions of the fitted compounds can be attributed to noise or uncertainties in the XANES data, or to the distortion of XANES spectra compared to the bulk when in nanosized regions. Large divergences between the two LCF methods could signal the absence of some references. Notably, the largest deviation between the two methods was observed for FB1, hinting at a potential missing reference for this type of ash.

3.3. Qualitative analysis of EXAFS data

EXAFS data was measured for three ash samples: GB4, GB5, and the GB4 ash stored at 75 % RH under 5 months. The EXAFS data are here used qualitatively, indicating the type of atomic environment around the probing atom, here zinc, and the degree of its disorder.

In Fig. 4, the Fourier transformed (FT) EXAFS data for the ashes (lower panel) and a selection of relevant references (upper panel) are plotted. For comparison, the EXAFS spectra, derived from summing the EXAFS spectra of the references according to the proportional weights from the XANES LCF, is shown as dashed lines in the lower panel. From the upper panel in Fig. 4, it can be seen that the Zn-Cl distance ($ZnCl_2$, K_2ZnCl_4, $KZnCl_3$, and $CaZnCl_4$) is significantly longer than that for Zn-O (closest neighbor in most other references). In the FT EXAFS spectra of the fresh ash, the r for the 1st shell confirms the initial presence of the alkali zinc chlorides in the ash. For the aged ash (75 % RH), there is a shift in r of the 1st shell compared to the raw ashes, as would be expected if the alkali zinc chloride is transformed into $Zn_5(OH)_8Cl_2 \cdot H_2O$ when the ash is stored at 75 % RH, further discussed in Section 3.6.

Apart from the average distance to the nearest neighbors of the zinc, EXAFS can also give information about long-range ordering, manifested in EXAFS as high frequency contributions in the FT spectra at large distances. As expected, the ash EXAFS spectra estimated from a linear combination of the references, inherently display a more pronounced degree of structural ordering compared to the measured ash EXAFS spectra reflecting the characteristics of the bulk reference materials.
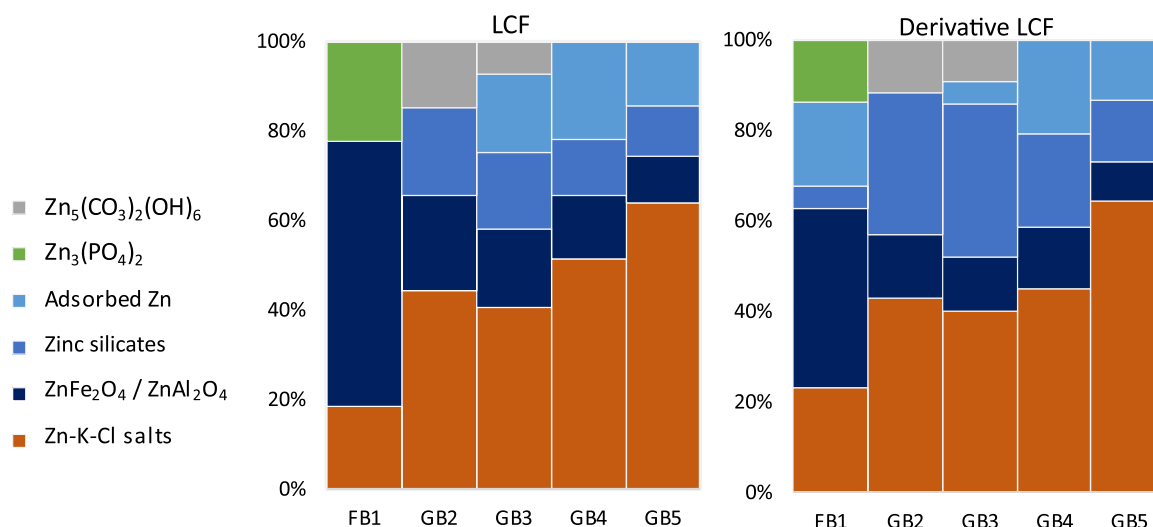

Fig. 3. Results from the LCF: in the left panel results from fitting the normalized XANES spectra and in the right panel the results from fitting the normalized derivative. In both graphs, the y-axis corresponds to the percentage of zinc in the specific chemical form.
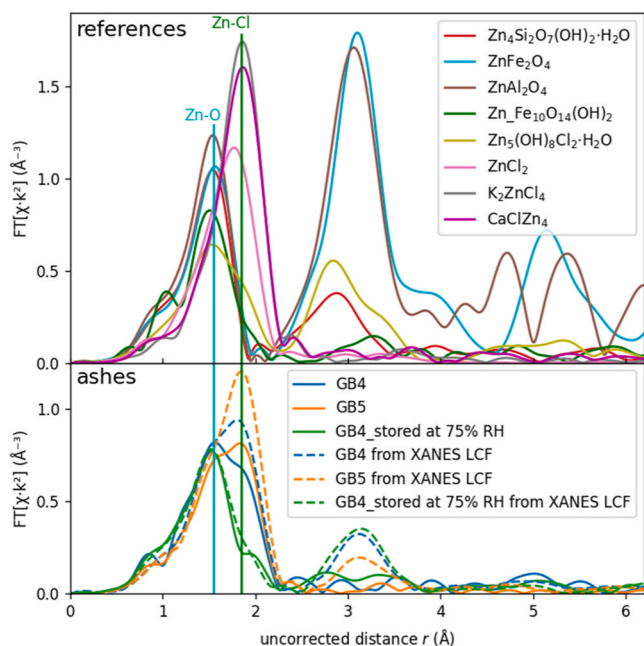
Fig. 4. Experimental Fourier transformed EXAFS spectra of references (top) and ashes (bottom, solid lines). The linear combination weights obtained from XANES spectra were also applied to EXAFS spectra of the references; shown as dashed lines in the bottom plot. The plot supports the result from the XANES spectra that alkali-zinc-chlorides are present in the fresh ash and disappears as the ash is aged.

Additionally, FT EXAFS peaks of highly ordered atomic shells are narrow and, reversely, disordered shells have broadened FT contributions.

3.4. Nano-XANES analysis

Among the 20 XANES spectra analyzed, four exhibited distinct similarities to zinc spinels – three corresponding to $ZnFe_2O_4$ and one to $ZnAl_2O_4$, substantiating the presence of these zinc spinels in the coarse fraction of the ash particles. These spectra are displayed alongside the spectra of $ZnFe_2O_4$ and $ZnAl_2O_4$ in Fig. 5. The observed disorder compared to the pure references is likely attributable to the presence also of other forms in the relatively thick ash particles (the analyzed volume is a cylinder with a diameter of 50 nm that extends through the entirety of the particle). All spectra are shown in the SI, Fig. S2. In each point, the elemental composition is measured by XRF, presented in SI, Table S3. As expected, the points for which the nano-XANES resembles $ZnFe_2O_4$ are rich in Fe. Note that the elemental analysis is restricted to elements heavier than aluminium and lighter than gallium.

Given that neither $ZnFe_2O_4$ nor $ZnAl_2O_4$ in the fly ash are products of condensation processes, it is inferred that these particles likely originate as fragments transported from the incineration bed entrained in the flue gas. This hypothesis might also elucidate the heightened prevalence of these compounds in the FB1 ash [33].

3.5. Sequential leaching

The full result from the sequential leaching is shown in Fig. S1 in SI. In short, 60–73 % of the zinc in the GB ashes was extracted in the first steps of the sequence (until step "A5", i.e. soluble in water and weak acid), while the corresponding fraction in the FB ash was somewhat lower (47 %). The fraction released in the reducing extraction ("Red") amounted to 10–20 % for all samples, while only very small amounts were extracted under oxidative conditions ("Ox"), which is expected given the origin of the samples (ash formed in an oxygen rich environment). Furthermore, a total of 10–15 % of the zinc contents remained
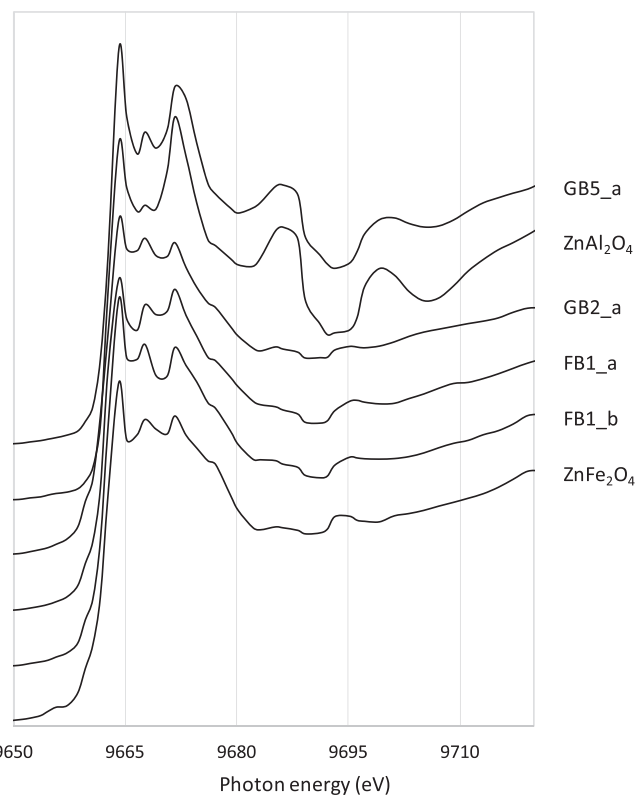
insoluble throughout the sequence for all GB ashes, while this inert fraction was higher for the FB ash (~30 %).

Although sequential leaching does not provide direct information about chemical speciation, the results can be used as a complement to XANES data. Plotting the zinc fraction leached in steps "MQ", "Ac7" and "Ac5" against the fraction of zinc in the form of alkali zinc chloride salts, carbonates, and phosphate, shows a clear correlation (circles in Fig. 6), thus supporting the results from XANES LCF. Adding the zinc fraction identified as zinc adsorbed to surfaces (Zn_ferrihydrite), this correlates well with the extracted fraction up until step *iv* ("Red"), shown as diamonds in Fig. 6. Note that the full speciation from XANES is uncertain for FB1, likely explaining the lower correlation for this ash. The leaching results indicate that the zinc bound as spinels was overestimated for the FB1 ash.

3.6. Chemical transformations of zinc during storage

To further investigate observed changes in zinc speciation over time in the prepared samples, and to disentangle impact of exposure to oxygen, water vapor, and the creation of new surfaces by grinding, a test was designed storing a subset of samples of the GB4 ash for five months, under six different conditions given in Table 2 and described in Section 2.6.

The most pronounced transformation was observed in the sample keept at 75 % RH. The sample stored in a fully packed airtight vial ("raw ash" in Fig. 7) showed no alteration in zinc speciation during the storage. This suggests that when stored in this way after collection, the transformation in speciation of the ash is kept to a minimum. While the effect of grinding appeared marginal, the results reveal a subtle yet distinct variance in the XANES spectra of ground and unground samples stored under identical conditions. Small but noticeable shifts in the XANES spectra were observed for both the samples stored at low humidity (<20 % RH) in air and in an atmosphere of nitrogen (N_2). The parallel
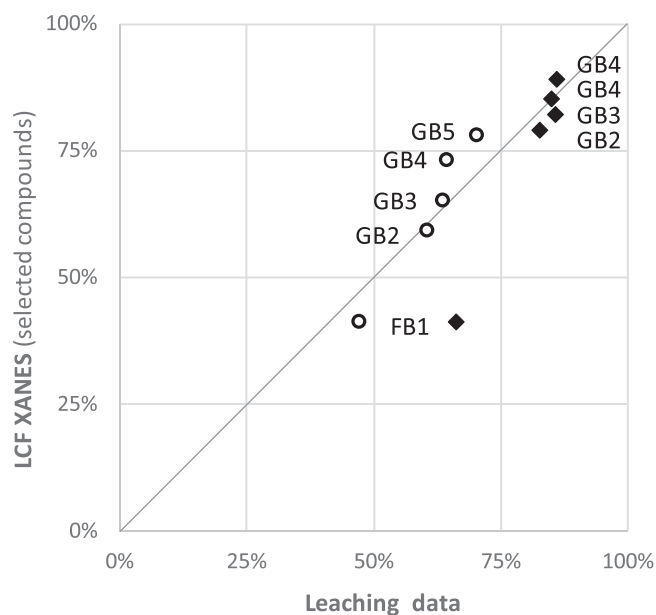

Fig. 5. Selected nano-XANES spectra closely resembling $ZnFe_2O_4$ and $ZnAl_2O_4$ and the corresponding XANES reference spectra of the pure compounds measured also with nano-XANES.

Fig. 6. Circles represent the correlation between the zinc-fraction leaching in the three first steps ("MQ", "Ac7", and "Ac5") with zinc predicted by XANES to be in the form of alkali-zinc-salts and as carbonates and phosphates. Diamonds represent the correlation with zinc leaching up till the 4th step ("MQ", "Ac7", "Ac5", and "Red") with zinc predicted to be in forms now also including zinc adsorbed to surfaces/as ferrihydrites.

transformation of both samples implies that changes might be attributed to exposure during handling rather than the storage conditions.

The XANES spectra for the samples stored at the various conditions are shown in Fig. 7 (left panel). The major change in the XANES features upon storage at 75 % RH was for the peak ~9664.4 eV, decreasing in intensity while the broad feature ~9668 eV increased in intensity (indicated by grey arrow in Fig. 7). The LCF of the XANES for the samples stored for five months indicates that the major change in XANES spectra is explained by hydroxylation of K_2ZnCl_4 into forming $Zn_5(OH)_8Cl_2 \cdot H_2O$. K_2ZnCl_4 is a hygroscopic salt that easily takes up water vapor from the air. Proof of the formation of $Zn_5(OH)_8Cl_2 \cdot H_2O$ at basic conditions, although not in fly ash, is found in literature [34,35]. The results from the LCF are presented in the right panel of Fig. 7.

In the test only one GB ash was used. However, alteration of zinc speciation was discernible in all the prepared tablets of the fresh ashes upon reanalysis two months post-preparation. The extent of the
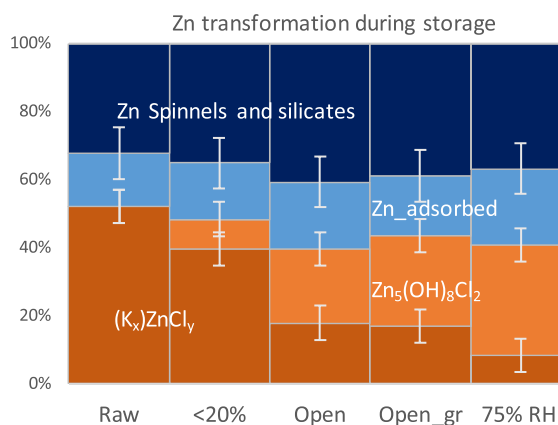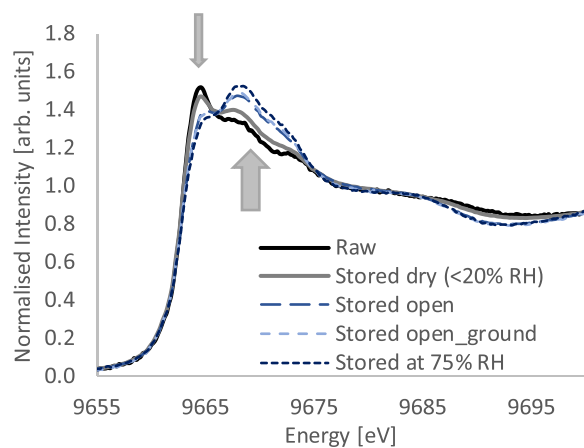
transformation was least pronounced in the FB ash, aligning well with the lower concentration of potassium zinc chlorides in the FB 1 ash.

In addition to zinc, we also examined the XANES spectra of other elements in the ash, namely chromium (Cr), copper (Cu), lead (Pb), and antimony (Sb). No corresponding change in speciation was observed for any of these elements.

3.7. Discussion and comparative analysis of the results with previous studies

Even though most earlier studies om waste incineration ash do not report any presence of K_2ZnCl_4 in the fly ash, it has been mentioned in a few studies [30,31]. While Zucha and colleagues [31] describe their finding as rare, they assert that their results are conclusive. In both the work of Zucha et al. [31] and of Bayuseno and Schmahl [30], X-Ray Diffraction (XRD) was used to identify the chemical form of zinc. The concentrations of K_2ZnCl_4 can be considered low for XRD in the complex ash matrix. As an example, Chen et al. [36] suggest that a zinc-phase needs to comprise at least 2 wt% of the sample to be identifiable via XRD. Our findings support that K_2ZnCl_4 is initially formed in the fly ash, and that this in fact is the dominating form of zinc in the GB ashes here investigated (40–64 %).

Although previous research has employed XANES to investigate the chemical forms of zinc in fly ash from WtE facilities [16,18,37], to the best of our knowledge, this study is the first to confirm the presence of potassium zinc chlorides. Earlier studies do report presence of $ZnCl_2$, but in typically lower ratios than here reported. This might be attributed to the fact that no earlier XANES studies includes alkali zinc chlorides as references. However, the very characteristic white line at the zinc K-edge of the zinc alkali chloride salts would lead to clear discrepancies between the ash spectra and the linear combination of the references suggested, which is not the general case. A possible explanation for this is that the zinc already had undergone a chemical transformation into Simonkolleite ($Zn_5(OH)_8Cl_2 \cdot H_2O$), here shown to occur during dry storage, and accelerated by the typical sample preparation procedure used for XAS (grinding, mixing with binder and pressed into tablets).

In [30] it is hypothesized that the K_2ZnCl_4 initially observed in their ash samples was transformed into Gordaite ($NaZn_4(SO_4)(OH)_6Cl \cdot (H_2O)_6$) upon hydration. This observation is in-line with the observation in the current study, but we here find that the compound formed is Simonkolleite ($Zn_5(OH)_8Cl_2 \cdot H_2O$). Simonkolleite is, according to an earlier study in corrosion science of zinc [38], a first reaction product before transformed into Gordaite under certain conditions. This suggests that Gordaite could be formed also in the ash over time if water is available. Simonkolleite and Gordaite are, contrary to K_2ZnCl_4,

Fig. 7. The normalized XANES spectra of the zinc K-edge of the fresh and aged fly ash from GB4 (left panel), and results from the linear combination fitting of the XANES spectra. The y-axis corresponds to the percentage of zinc in the specific chemical form. Features in the XANES spectra decreasing/increasing with aging indicated by grey arrows.

non-soluble in water, while soluble in acidic solutions [35]. Thus, the transformation could reduce leaching into the environment.

In our study, we identified the presence of zinc-bearing spinels, namely $ZnAl_2O_4$ and $ZnFe_2O_4$, within the analyzed ash samples. These spinels account for 10–20 % of the total zinc content in the GB ash, and a significantly higher proportion in the fly ash from the FB. Moreover, detailed nano-resolved XANES analysis provides incontrovertible evidence for the existence of $ZnAl_2O_4$ and $ZnFe_2O_4$ in particles larger than 2 μm, where areas of almost pure $ZnAl_2O_4$ and $ZnFe_2O_4$ were identified. Thus, the nano-XANES data strengthens the theory that these spinel structures are primarily associated with the coarser particles in the fly ash, i.e. fragments transported from the incineration bed into the flue gas. The occurrence of zinc-bearing spinels aligns with findings from several prior studies (e.g., [16,18,33]).

The results of the present study propose the presence of hemimorphite (up to 20 %), a hydrated form of willemite [39]. This discovery aligns with findings from our previous study [16], also supported by studies of char [40], while contrasting with others that have identified zinc predominantly in the form of willemite (e.g. [17,37]). However, the contrasting studies did not include hemimorphite as a reference compound for LCF of the XANES data. A study by de Matteis and co-authors [41] suggests that the presence of hemimorphite could be a misinterpretation of zinc in silicate glass. This is a plausible hypothesis taken that the hemimorphite was found also in the fresh non-hydrated ashes. However, both zinc bearing forms have similar leaching properties and toxicity.

Struis et al. [17] performed a study on the effect on the speciation of zinc with heat treatment of ash using XAS (EXAFS), including a relatively extensive library of references. Their results show that the untreated ash was composed of ~60 % by $Zn_5(OH)_6(CO_3)_2$. This is higher than what was found in any of the ashes here analyzed (< 14 %). However, their references did not include any alkali zinc chlorides, nor hydroxylated zinc chlorides. In their study, around 40 % of the zinc was counted as inert, according to the EXAFS results composed by Zn_2SiO_4 and $ZnAl_2O_4$, in a ratio of (3:1).

Bayuseno and Schmahl [30] suggest that zinc in the WtE ash also occurs in the form of wurtzite ((Zn,Fe)S), or in some other amorphous phase. An earlier XANES study of two ZnS polytypes (cubic and hexagonal) shows that the XANES K-edge spectra of the two polytypes are indistinguishable [42]. In the current study, ZnS (cubic) was included as a reference, and our results do not indicate any presence of ZnS in the fresh ash, as expected in the highly oxidative environment prevalent within the fly ash.

The prediction of $Zn_3(PO_4)_2$ (here in the FB ash) was not reported earlier. However, a study on bottom ash [43] suggests cationic substitution of Zn^{2+} in $Ca_3(PO_4)_2$, supporting our finding. Such highly local chemical environments add a layer of complexity when understanding the chemical state within ash matrices and underscore the need for further studies to thoroughly comprehend the various chemical forms of zinc present in the ash.

The fly ash collected by the electrostatic precipitator is a mix of two types of particles, coarse solid particles entrained from the combustion bed (typically larger than a few micrometers) and particles formed from the gas phase condensation (nucleation). The latter are typically in the size range from some nm up to a few hundreds of nm. The abundance of the particles formed by nucleation depends on the available surface of existing particles for condensation [44,45]. The alkali zinc salt is anticipated to arise through a condensation process, whereas the zinc-containing silicates, zinc ferrite, and zinc aluminate likely originate from particles entrained from the combustion bed. This entrainment is believed to be more pronounced in the case of FB [33] which aligns with our observation of a heightened presence of zinc ferrite and zinc aluminate in the FB1 ash. In the current study no size specific analysis of particles was possible since fragmentation of the filter ash particles would require high energy to consistently de-aggregate the submicron particles.

To our knowledge, there are still very few studies focused on the speciation details of particles present and formed in the flue gas during WtE incineration. Such details could be the key to more efficient and safe utilization of fly ash, today most often classified as hazardous waste.

3.8. XAS for speciation of trace metals in ash

X-ray Absorption Spectroscopy (XAS) presents a significant advantage in its ability to scan the absorption edge of a specific element, effectively probing the chemical form of the target atom while remaining unaffected by other compounds present. The technique offers a unique perspective on the local chemical environment of the target atom also in the absence of long-range order [46], including zinc adsorbed to surfaces or zinc involved in cation substitution (forming solid solutions). Moreover, XAS is capable of probing both amorphous and crystalline phases, altogether making it a particularly powerful tool in determining the chemical forms of trace elements in WtE incineration ash.

XANES analysis is empirical in nature, most often done via comparison to XANES spectra of reference compounds [47]. Thus, the efficacy of XANES analysis relies heavily on the use of a comprehensive and relevant reference library of XANES spectra. Recognizing this need, we have developed a unique and extensive library of zinc references. This library, encompassing over 30 compounds, is tailored to the nuances of zinc chemistry within the specific context of fly ash, thereby enhancing the precision and relevance of the analysis. The references include zinc absorbed to surfaces, i.e. to ferrihydrite, $CaCO_3$, $CaSO_4$, and bentonite, whereof the first is predicted to be present in the GB ashes. Zinc's strong affinity for binding to the surfaces of iron oxides has been shown in many studies on zinc in soils (e.g. [48]), and zinc adsorbed to ferrihydrite has been reported in one earlier study by Pattanaik et al. [49] on incineration ash.

In this study, the LCF consistently predicted the presence of the same set of Zn compounds in the ash samples out of the 32 references. This is an indication that the fit is robust and includes the major relevant references. To investigate this further, both the normalized XANES spectra and derivative of these were fitted. This dual approach would indicate if a pertinent reference was missing through considerable deviations in the result from respective approach.

To further ensure the accuracy of the results from XANES, it is advisable to compare them with those obtained from complementary techniques. In this study including EXAFS, nano-XANES, and sequential leaching. Although sequential leaching does not directly reveal speciation, it remains a widely used method for understanding leaching dynamics and is linked to zinc speciation.

As the atomic distance of zinc and chloride is significantly different to that of zinc and oxide, EXAFS could in this study be used to confirm that zinc was initially partly bound to a chloride atom. Apart from information about neighboring atoms, EXAFS provides information about long-range ordering. In this study the fly ash displayed a low degree of structural ordering and thus, LCF of EXAFS is likely not very suitable for these ashes.

4. Conclusion

Zinc speciation was investigated in fly ash sourced from MSWI using primarily XANES, interpreted against a library of over 30 pertinent reference compounds. The zinc forms identified in the grate-fired boiler (GB) ash (the most common technology for WtE incineration) were similar across all four samples analyzed. The zinc forms in the ash from the circulating fluidized bed boiler (FB) was somewhat deviant.

The predominant zinc form present in the fresh ash was potassium zinc chloride, most probably K_2ZnCl_4 formed in the condensates, corresponding to 41–64 % of the zinc in the GB fly ashes, while ~20 % in the FB ash. For the FB ash, the most common zinc bearing compounds were $ZnFe_2O_4$ and $ZnAl_2O_4$, corresponding to ~60 % of the zinc in the ash, while only 10–21 % in the GB ash. The presence of $ZnFe_2O_4$ and

$ZnAl_2O_4$ was confirmed by nano-resolved XANES, showing areas in the coarse particles that were entirely dominated by these forms. In addition, zinc in the form of $Zn_4Si_2O_7(OH)_2 \cdot H_2O$, $Zn_5(CO_3)_2(OH)_6$, and Zn adsorbed to the surfaces of iron oxides were found in the GB ashes. For the FB ash the XANES results also indicate presence of $Zn_3(PO_4)_2$. EXAFS data for selected samples indicate that the ash exhibits a lower degree of structural order compared to reference materials, suggesting that ordered regions may be localized around the target atom.

We show that when exposed to humidity in the air, K_2ZnCl_4 is hydroxylated and transformed into Simonkolleite ($Zn_5(OH)_8Cl_2 \cdot H_2O$) in the strongly alkaline ash. The study demonstrates that the humidity in the air is sufficient to trigger this transformation in zinc speciation, a change also induced by the conventional sample preparation protocols for XAS, possibly due to H_2O in binder media. Thus, studies of zinc speciation in pristine ash requires storing the samples at low RH prior to the analyses.

CRediT authorship contribution statement

Tone Klufthaugen: Writing – review & editing. **Simone Sala:** Writing – review & editing, Investigation, Data curation. **Inge Johansson:** Writing – review & editing, Project administration, Funding acquisition, Conceptualization. **Jenny Rissler:** Writing – review & editing, Writing – original draft, Visualization, Validation, Methodology, Investigation, Funding acquisition, Formal analysis, Data curation, Conceptualization. **Karin Karlfeldt Fedje:** Writing – review & editing, Investigation, Funding acquisition, Conceptualization. **Charlotte Nilsson:** Writing – review & editing, Methodology, Data curation. **Haakon Rui:** Writing – review & editing, Methodology. **Konstantiv Klementiev:** Writing – review & editing, Formal analysis, Data curation. **Burcak Ebin:** Writing – review & editing, Methodology, Data curation.

Declaration of Competing Interest

The authors declare that they have no known competing financial interests or personal relationships that could have appeared to influence the work reported in this paper.

Data availability

Data will be made available on request.

Acknowledgements

Environmental implication

Fly ash from municipal solid waste incineration is classified as hazardous waste due to the content of potentially toxic elements like zinc. For zinc it is not the elemental content per se that determines the toxicity but the speciation. At the same time, the ash matrix is complex and traditional methods are limited in analyzing the speciation of metals in low concentrations in the ash. Synchrotron-based techniques like XAS have been identified as important, but the analysis relies on relevant reference libraries. This study is focused on zinc speciation in five fly ashes produced in plants under normal incineration conditions.

Appendix A. Supporting information

Supplementary data associated with this article can be found in the online version at doi:10.1016/j.jhazmat.2024.135203.

References

[1] Eurostat, Derived 2023-10–01 (Last data update: 21/08/2023) Euro Stat Statistics explained; Municipal waste statistics, ⟨https://ec.europa.eu/eurostat/statistics-explained/index.php?title=Municipal_waste_statistics#Municipal_waste_generation⟩.

[2] Alterary, S.S., Marei, N.H., 2021. Fly ash properties, characterization, and applications: a review. ISSN 1018-3647 J King Saud Univ - Sci Volume 33 (6), 101536. https://doi.org/10.1016/j.jksus.2021.101536.

[3] Zhang, Y., Wang, L., Chen, L., Ma, B., Zhang, Y., Ni, W., Tsang, D.C.W., 2021. Treatment of municipal solid waste incineration fly ash: state-of-the-art technologies and future perspectives. ISSN 0304-3894 J Hazard Mater Volume 411, 125132. https://doi.org/10.1016/j.jhazmat.2021.125132.

[4] Nedkvitne, E.N., Borgan, Ø., Øistein Eriksen, D.Ø., Rui, H., 2021. Variation in chemical composition of MSWI fly ash and dry scrubber residues. ISSN 0956-053X Waste Manag 126, 623–631. https://doi.org/10.1016/j.wasman.2021.04.007.

[5] European Commission, Internal Market, Industry, Entrepreneurship and SMEs, Derived 2024-01–08. Critical Raw Materials Act, ⟨https://single-market-economy.ec.europa.eu/sectors/raw-materials/areas-specific-interest/critical-raw-materials/critical-raw-materials-act_en⟩.

[6] Chandler, A.J., Eighmy, T.T., Hartlén, J., Hjelmar, O., Kosson, D.S., Sawell, S.E., Sawell, S.E., van der Sloot, H.A., AHAVehlow, J., 1997. Municipal Solid Waste Incinerator Residues. Elsevier,, Amsterdam; New York.

[7] Fedje, K.K., Andersson, S., 2022. Zinc recovery from Waste-to-Energy fly ash—A pilot test study. Waste Manag 118, 90–98. https://doi.org/10.1016/j.wasman.2020.07.017.

[8] Rasmusen, E., 2015. Sambehandling af RGA og scrubber væske fra forbrændingsanlæg med HALOSEP processen, Miljøprojekt nr. 1648, Danish EPA (Miljøstyrelsen), ⟨https://www2.mst.dk/Udgiv/publikationer/2015/02/978–87-93283–72-5.pdf⟩.

[9] Schlumberger, S., Schuster, M., Ringmann, S., Koralewska, R., 2007. Recovery of high purity zinc from filter ash produced during the thermal treatment of waste and inerting of residual materials. Waste Manag Res 25, 547–555. https://doi.org/10.1177/0734242×07079870.

[10] Bakke, P., 2018. Extraction of metal products from MSWI fly ash., 4th Hydrometallurgy Seminar, Oslso, Norway https://hydromet.no/Presentasjoner/Oslo%202018/Norsep%20Hydromet%20ed.pdf.

[11] Karlfeldt Fedje, K., Andersson, S., Modin, O., Frändegård, P., Pettersson, A., 2014. Opportunities for Zn recovery from Swedish MSWI fly ashes, SUM 2014. Second Symposium on Urban Mining. CISA Publisher, Italy,, Bergamo, Italy.

[12] Grünert, W., Klementiev, K., 2020. X-ray absorption spectroscopy principles and practical use in materials analysis. Phys Sci Rev 5 (4), 20170181. https://doi.org/10.1515/psr-2017-0181.

[13] van Bokhoven, J.A., Lamberti, C., 2016. X-Ray absorption and X-Ray emission spectroscopy: theory and applications. John Wiley & Sons Ltd,, Chichester (UK). https://doi.org/10.1002/9781118844243.

[14] Hsiao, M.C., Wang, H.P., Wei, Y.L., Chang, J.-E., Jou, C.J., 2002. Speciation of copper in the incineration fly ash of a municipal solid waste. J Hazard Mater 91, 301–307. https://doi.org/10.1016/s0304-3894(02)00015-8.

[17] Struis, R., Ludwig, C., Lutz, H., Scheidegger, A., 2004. Speciation of zinc in municipal solid waste incineration fly ash after heat treatment: an x-ray absorption spectroscopy study. Environ Sci Technol 38, 3760–3767. https://doi.org/10.1021/es0346126.

[18] Takaoka, M., Yamamoto, T., Takeda, N., Oshita, K., Uruga, T., 2005. Direct speciation of lead, zinc and antimony in fly ash from waste treatment facilities by XAFS spectroscopy. T115 Phys Scr 943–945. https://doi.org/10.1238/Physica.Topical.115a00943.

[20] Tuan, Y.-J., Paul Wang, H., Chang, J.-E., Chao, C.-C., Tsai, C.-K., 2010. Speciation of copper in the thermally stabilized slag. Nucl Instrum Methods Phys Res, Sect A 619, 316–318. https://doi.org/10.1016/j.nima.2010.01.023.

[15] Lassesson, H., Steenari, B.-M., 2013. Speciation of copper in ash from a fluidized-bed boiler fired with municipal solid waste. Energy Fuels 27, 3891–3897. https://doi.org/10.1021/ef400386j.

[19] Tian, S., Zhu, Y., Meng, B., Guan, J., Nie, Z., Die, Q., Xu, W., Yu, M., Huang, Q., 2018. Chemical speciation of lead in secondary fly ash using X-ray absorption spectroscopy. Chemosphere 197, 362–366. https://doi.org/10.1016/j.chemosphere.2018.01.026. PMID: 29407806.

[16] Rissler, J., Klementiev, K., Dahl, J., Steenari, B.-M., Edo, M., 2020. Identification and quantification of chemical forms of Cu and Zn in MSWI ashes using XANES. Energy Fuels 34 (11), 14505–14514. https://doi.org/10.1021/acs.energyfuels.0c02226.

[21] Newville, M., 2014. Fundamentals of XAFS. Rev. Mineral. Geochem. 78 (1), 33–74. https://doi.org/10.2138/rmg.2014.78.2.

[22] Klementiev, K., Norén. K., Carlson, S., Sigfridsson Clauss, K.G.V., Persson, I., 2015. The BALDER Beamline at the MAX IV Laboratory. Journal of Physics: Conference Series, 712, 16th International Conference on X-ray Absorption Fine Structure (XAFS16) 23–28, Karlsruhe, Germany. doi:10.1088/1742–6596/712/1/012023.

[23] Ravel, B., Newville, M., 2005. ATHENA, ARTEMIS, HEPHAESTUS: data analysis for X-ray absorption spectroscopy using IFEFFIT. J Synchrotron Radiat 12, 537–541. https://doi.org/10.1107/S0909049505012719.

[24] Klementiev, K.V., 2001. Deconvolution problems in X-ray absorption fine structure spectroscopy. J Phys D: Appl Phys 34, 209–217. https://doi.org/10.48550/arXiv.physics/0101105.

[25] Chen, D.T., Roy, A., Li, Y.Q., Bogush, A., Au, W.Y., Stegemann, J.A., 2023. Speciation of toxic pollutants in Pb/Zn smelter slags by X-ray Absorption Spectroscopy in the context of the literature. ISSN 0304-3894 J Hazard Mater 460, 132373. https://doi.org/10.1016/j.jhazmat.2023.132373.

[26] Quinn, P.D., Alianelli, L., Gomez-Gonzalez, M., Mahoney, D., Cacho-Nerin, F., Peach, A., Parker, J.E., 2021. The Hard X-ray nanoprobe beamline at diamond light source. J Synchrotron Radiat 28, 1006–1013. https://doi.org/10.1107/S1600577521002502.

[27] Karlsson, S., Allard, B., Håkansson, K., 1987. Characterisation of stream bed sediments receiving high loadings of acid mine effluents. Chem Geol 67, 1–15. https://doi.org/10.1016/0009-2541(88)90002-2.

[28] Tessier, A., Campbell, P., Bisson, M., 1979. Sequential extraction procedure for the speciation of particulate trace metals. Anal Chem 51, 844–851. https://doi.org/10.1021/ac50043a017.

[29] Greenspan, L., 1977. Humidity fixed points of binary saturated aqueous solutions. J Res Natl Inst Stand Technol, Jan-Feb 81A (1), 89–96. https://doi.org/10.6028/jres.081A.011.

[30] Bayuseno, A.P., Schmahl, W.W., 2011. Characterization of MSWI fly ash through mineralogy and water extraction. ISSN 0921-3449 Resour, Conserv Recycl 55 (5), 524–534. https://doi.org/10.1016/j.resconrec.2011.01.002.

[31] Zucha, W., Weibel, G., Wolffers, M., Eggenberger, U., 2020. Inventory of MSWI fly ash in Switzerland: heavy metal recovery potential and their properties for acid leaching. Processes 8, 1668. https://doi.org/10.3390/pr8121668.

[32] Gomes, A., Azevedo, G.M., Depeyrot, J., Mestnik-Filho, J., da Silva, G.J., Tourinho, F.A., Perzynski, R., 2011. ZnFe2O4 nanoparticles for ferrofluids: a combined XANES and XRD study. ISSN 0304-8853 J Magn Magn Mater 323 (10), 1203–1206. https://doi.org/10.1016/j.jmmm.2010.11.006.

[33] Staničić, I., Cañete Vela, I., Backman, R., Maric, J., Cao, Y., Mattisson, T., 2021. Fate of lead, copper, zinc and antimony during chemical looping gasification of automotive shredder residue. ISSN 0016-2361 Fuel 302, 121147. https://doi.org/10.1016/j.fuel.2021.121147.

[34] Li, Y., Zou, Y., Hou, Y., 2011. Synthesis and characterization of simonkolleite nanodisks and their conversion into ZnO nanostructures. Cryst Res Technol 46 (3), 305–308. https://doi.org/10.1002/crat.201000673.

[35] McMahon, M.E., Santucci, R.J.Jr, Scully, J.R., 2019. Advanced chemical stability diagrams to predict the formation of complex zinc compounds in a chloride environment. RSC Adv (35). https://doi.org/10.1039/C9RA00228F.

[36] Chen, D.T., Au, W.Y., van Ewijk, S., Roy, A., Stegemann, J.A., 2021. Elemental and mineralogical composition of metal-bearing neutralisation sludges, and zinc speciation – A review. ISSN 0304-3894 J Hazard Mater 416, 125676. https://doi.org/10.1016/j.jhazmat.2021.125676.

[37] Cai, X., Huang, Qx, Alhadj-Mallah, Mm, Chi, Y., Yan, J.H., 2015. Characterization of zinc vapor condensation in fly ash particles using synchrotron X-ray absorption spectroscopy. J Zhejiang Univ-Sci A 16, 70–80. https://doi.org/10.1631/jzus.A1400178.

[38] Odnevall, I., Leygraf, C., 1993. Formation of NaZn4Cl(OH)6SO4·6H2O in a marine atmosphere. Corros Sci 34 (8), 1213–1229. https://doi.org/10.1016/0010-938X(93)90082-R.

[39] Vanaecker, M., Courtin-Nomade, A., Bril, H., Laureyns, J., Lenain, J.F., 2014. Behavior of Zn-bearing phases in base metal slag from France and Poland: A mineralogical approach for environmental purposes. J Geochem Explor 136, 1–13. https://doi.org/10.1016/j.gexplo.2013.09.001.

[40] Qian, T., Wang, Y., Fan, T., Fang, G., Shou, D., 2016. A new insight into the immobilization mechanism of Zn on biochar: the role of anions dissolved from ash. Sci Rep 6, 33630. https://doi.org/10.1038/srep33630.

[41] De Matteis, C., Pollastri, S., Mantovani, L., Tribaudino, M., 2024. Potentially toxic elements speciation in bottom ashes from a municipal solid waste incinerator: A combined SEM-EDS, µ-XRF and µ-XANES study. Environ Adv 15, 100453. https://doi.org/10.1016/j.envadv.2023.100453.

[42] Gilbert, B., Frazer, B.H., Zhang, H., Huang, F., Banfield, J.F.D., Lang, H.J.C., Srajer, G., De Stasio, G., 2002. X-ray absorption spectroscopy of the cubic and hexagonal polytypes of zinc sulfide. Phys Rev B 66, 245205.

[43] Falk, J., Hannl, T.K., Skoglund, N., Backman, R., Öhman, M., 2022. Thermodynamic equilibrium study on the melting tendency of the K-Ca-Mg-P-Si-O system with relevance to woody and agricultural biomass ash compositions. Energy Fuels 36 (13), 7035–7051. https://doi.org/10.1021/acs.energyfuels.2c00785.

[44] Brunner, T., Joeller, M., Obernberger, I., Frandsen, F., 2002, Aerosol and fly ash formation in fixed bed biomass combustion systems using woody biofuels, 12th European Conference and Technology Exhibition on Biomass for Energy, Industry and Climate Protection 17–21 June 2002, Amsterdam.

[45] Obernberger, I., 2009, Reached Developments of Biomass Combustion Technologies and Future Outlook. In: Proc. of the 17th European Biomass Conference, June 2009, Hamburg, Germany, ISBN 978–88-89407–57-3, pp.20–37, ETA-Renewable Energies (Ed.), Florence, Italy.

[46] Henderson, G.S., De Groot, F.M., Moulton, B.J., 2014. X-ray absorption near-edge structure (XANES) spectroscopy. Rev Mineral Geochem 78 (1), 75–138. https://doi.org/10.2138/rmg.2014.78.3.

[47] Waychunas, G.A., Fuller, C.C., Davis, J.A., 2002. Surface complexation and precipitate geometry for aqueous Zn (II) sorption on ferrihydrite I: X-ray absorption extended fine structure spectroscopy analysis. Geochim Et Cosmochim Acta 66 (7), 1119–1137. https://doi.org/10.1016/S0016-7037(01)00853-5.

[48] Van Eynde, E., Hiemstra, T., Comans, R.N.J., 2022. Interaction of Zn with ferrihydrite and its cooperative binding in the presence of PO4. ISSN 0016-7037 Geochim Et Cosmochim Acta 320, 223–237. https://doi.org/10.1016/j.gca.2022.01.010.

[49] Pattanaik, S., Huggins, F.E., Huffman, G.P., 2018. Variability of zinc speciation in fine particulate matter emitted from a boiler and a combustor using residual oils. ISSN 1352-2310 Atmos Environ 188, 185–191. https://doi.org/10.1016/j.atmosenv.2018.05.045.